Melting and Evaporation of Hydrometeors in Precipitation from the Anvil Clouds of Deep Tropical Convection[1]

COLLEEN A. LEARY[2] AND ROBERT A. HOUZE, JR.

Department of Atmospheric Sciences, University of Washington, Seattle 98195

(Manuscript received 21 August 1978, in final form 18 December 1978)

ABSTRACT

Five cases of horizontally uniform precipitation associated with anvil clouds were investigated using weather radar, rawinsonde, satellite and raindrop size data collected during the Global Atmospheric Research Program's Atlantic Tropical Experiment (GATE).

The area of horizontally uniform precipitation was in each case characterized by rainfall rates of 1–10 mm h^{-1}, in contrast to the 10–100 mm h^{-1} observed in convective cells. Concentrations of precipitation-sized ice particles above the melting layer and liquid water below the melting layer, together with observed particle spectra, suggest that aggregation occurs above the melting layer, and that riming occurs in sufficient amounts to produce graupel within the anvil cloud.

All five cases exhibited distinct radar bright bands in the melting layer. Cooling rates associated with the melting in this 1 km thick layer near the base of the anvil cloud were 1–7 K h^{-1}. These cooling rates were comparable to the 0.2–6 K h^{-1} cooling rates due to evaporation of raindrops below the melting layer, suggesting that melting as well as evaporation plays a role in the initiation and maintenance of a mesoscale downdraft beneath the anvil cloud.

1. Introduction

A prominent feature of some tropical weather systems of subsynoptic size and highly convective character is a thick layer of precipitating nimbostratus cloud, generally called the *anvil cloud*, which can extend from the 600–700 mb (3.2–4.4 km) level to about 200 mb (12.3 km) or above (Zipser, 1969, 1977; Houze, 1977). It usually forms several hours after deep convection first appears. The dynamical significance of the anvil cloud lies in mesoscale vertical air motions associated with its maintenance and the precipitation it produces. Mesoscale lifting within the anvil cloud has been proposed as a mechanism for its maintenance, and the presence of a mesoscale downdraft beneath the cloud base has been attributed to evaporative cooling of rain falling from the anvil cloud (Zipser, 1969, 1977; Houze, 1977; Brown, 1979).

Precipitation in and beneath the anvil cloud exhibits a characteristic signature when observed by radar. Its striking horizontal uniformity over a widespread area and its long duration are a sharp contrast to the strong horizontal gradients and vertical orientation of the short-lived echo patterns that accompany convective cells (Houze, 1975, 1977; Leary and Houze, 1979). Frequently, a narrow horizontal layer of high reflectivity called the *bright band* is observed just below the 0°C isotherm when the radar scans a vertical cross section through horizontally uniform precipitation.

In middle latitudes, horizontally uniform precipitation and radar bright bands are usually associated with extratropical cyclones, in which the major precipitation-producing mechanism is widespread lifting with vertical velocities on the order of tens of centimeters per second. There it is generally referred to as "stratiform" (Houghton, 1968) or "continuous" (Battan, 1973, pp. 185–195) precipitation. Only rarely has horizontally uniform precipitation been reported in convective systems in middle latitudes (e.g., Zwack and Anderson, 1970).

In the tropics, on the other hand, horizontally uniform precipitation has been observed in a wide variety of convective systems. Atlas *et al.* (1963) observed bright bands in the spiral rain bands of a hurricane. Biswas *et al.* (1962) and Ramana Murty *et al.* (1965) observed radar bright bands and horizontally uniform precipitation in monsoon precipitation over India. Zipser (1969, 1977) and Houze (1975, 1977) observed horizontally uniform precipitation in the rear portions of tropical squall-line systems, characterized by an arc-shaped leading edge, an oval-shaped cirrus shield at high levels, and a propagation speed of at least 5 m s^{-1} (Payne and McGarry, 1977; Houze and Cheng, 1977). Leary and Houze (1979) observed

[1] Contribution No. 482. Department of Atmospheric Sciences, University of Washington.

[2] Present affiliation: Atmospheric Science Group, Texas Tech University, Lubbock 79409.

0022-4928/79/040669-11$06.75

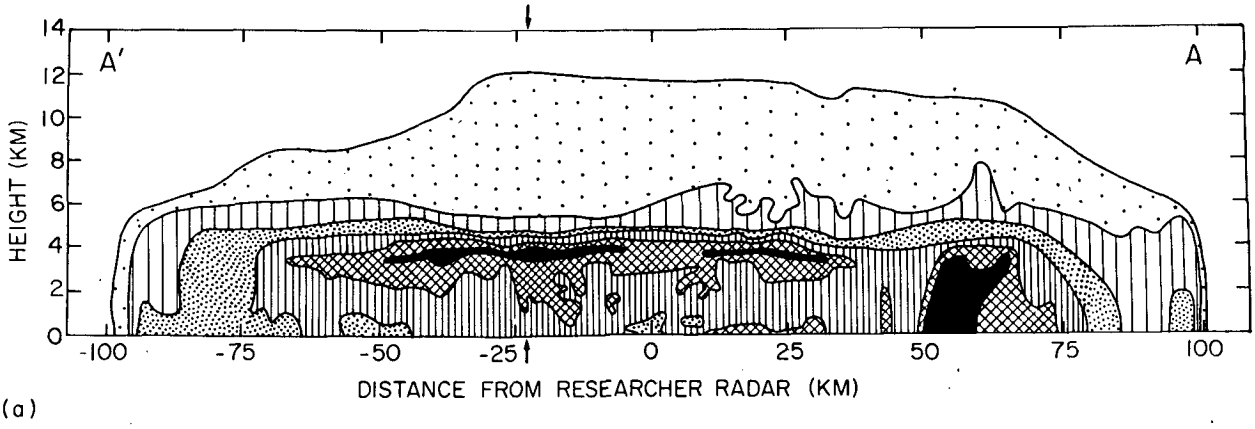

FIG. 1a. Vertical cross section derived from *Researcher* digital radar data for 2100 GMT 4 September 1974, lying along line A–A′ in Fig. 1b. The outside contour is for the minimum detectable echo, inner contours are for 23, 28, 33, 38 and 43 dBZ, and arrows indicate the vertical profile in Fig. 6a.

horizontally uniform precipitation and a radar bright band in the rear portions of intense mesoscale convective systems within a tropical cloud cluster that moved too slowly and were not well organized enough to be categorized as squall-line systems.

The ubiquity of horizontally uniform precipitation and pronounced radar bright bands associated with deep convection observed during the Global Atmospheric Research Program's Atlantic Tropical Experiment (GATE) (Houze, 1975, 1977; Leary and Houze, 1979) has led us to a detailed study of the microphysical processes in anvil cloud precipitation and their interactions with mesoscale dynamics. In particular, the location of the bright band near the base of the anvil cloud suggests that cooling due to melting of precipitation particles plays a role, along with evaporation, in initiating and maintaining the mesoscale downdraft beneath cloud base. This paper presents five examples of horizontally uniform precipitation and radar bright bands observed in tropical cloud clusters during GATE. We have used quantitative radar data, together with rawinsonde and satellite observations and measurements of raindrop size distributions, to synthesize a picture of the microphysical processes that accompany horizontally uniform precipitation in tropical cloud systems.

2. Data

a. Upper air observations

This study makes use of upper air observations (EDS, 1975) collected during GATE in their "Nationally Processed and Validated" form. As described by Acheson (1976), these include wind, temperature and humidity measurements at 5 mb intervals.

b. Radar observations

The GATE radar data have been described by Houze (1977). His Table 1 lists the characteristics of the four C-band radars, and his Fig. 1 illustrates the positions of the four ships carrying quantitative radars and indicates the overlapping coverage of the four radars. This study makes use of data from radars on board the *Researcher* and *Gilliss*. Each radar was operated in a three-dimensional scanning routine in which the antenna swept through 360° in azimuth for a series of elevation angles ranging from 0–30°. Signals returned to the radar were processed and recorded both photographically and digitally on board the ships. A complete set of sweeps required about 5 min. The horizontal and vertical cross sections in Figs. 1–5 and the vertical profiles in Fig. 6 were constructed from the digital form of the radar data.

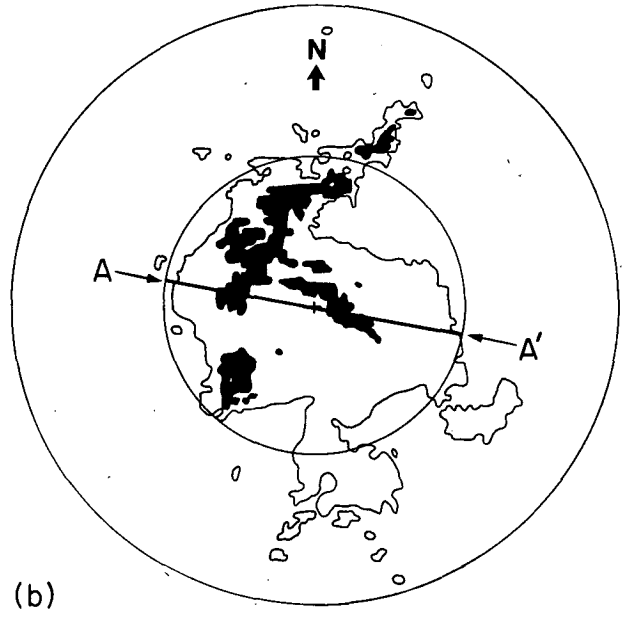

FIG. 1b. As in Fig. 1a except for horizontal cross section. The outside contour is for the minimum detectable echo, the inner contour is for 38 dBZ or 14 mm h^{-1}, and range marks are at 110 and 220 km.

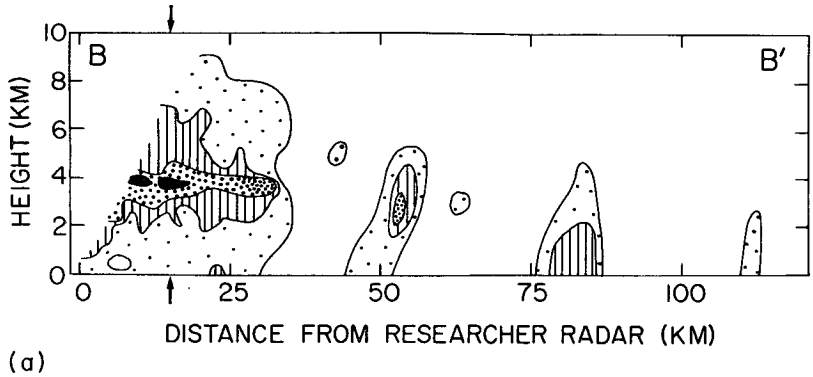

FIG. 2a. Vertical cross section derived from *Researcher* digital radar data for 0001 GMT 12 September 1974, lying along line B–B′ in Fig. 2b. The outside contour is for the minimum detectable echo, inner contours are for 23, 28 and 33 dBZ, and arrows indicate the vertical profile in Fig. 6b.

c. Satellite data

For this study, gridded SMS-1 satellite photographs and film loops were obtained through the *GATE Data Catalogue* (EDS, 1975), and special photographic data and contoured maps of the SMS-1 brightness intensity patterns for both infrared and sun-angle normalized visible images were prepared by the Space Science and Engineering Center at the University of Wisconsin.

d. Drop spectra measurements

A foil impactor operated at cloud-base level on board the NOAA DC-6 aircraft and disdrometers on board *Researcher* and *Gilliss* during GATE were used to obtain drop size distributions of precipitation-sized particles. The DC-6 and *Researcher* data have been described and tabulated by Cunning and Sax (1977a,b). The *Gilliss* disdrometer data have been described by Austin and Geotis (1979).

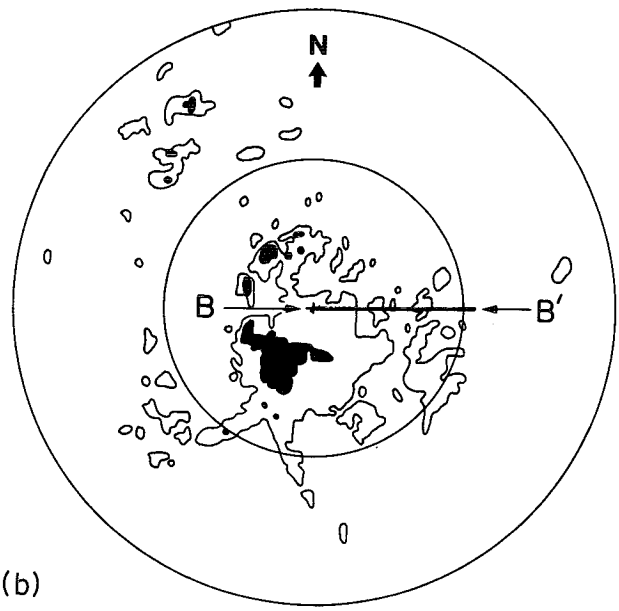

FIG. 2b. As in Fig. 2a except for horizontal cross section. The outside contour is for the minimum detectable echo, the inner contour is for 38 dBZ or 14 mm h^{-1}, and range marks are at 110 and 220 km.

3. Five examples of horizontally uniform reflectivity patterns and radar bright bands observed during GATE

In each of the cases shown in Figs. 1–5, the area of horizontally uniform precipitation developed in association with intense convective cells. In Figs. 1–4, the area of horizontally uniform precipitation occurred in the rear portions of four of the tropical squall-line systems described by Houze (1975), and in Fig. 5 it occurred in the rear portion of one of the intense non-squall convective systems described by Leary and Houze (1979).

Horizontally uniform precipitation in all five cases was distinctive on account of its widespread extent, long duration, and the absence of strong horizontal gradients of reflectivity. These characteristics contrast sharply with those of the precipitation in convective cells which have small horizontal dimensions (~1–100 km^2), short lifetime ($\lesssim$1 h), and vertically oriented contours of radar reflectivity. For example, compare in Fig. 3a the convective cell centered at a range of 140 km to the area of horizontally uniform precipitation extending from 20–45 km and from 50–85 km. The areas occupied by the five regions of horizontally uniform precipitation ranged from 1.0×10^4–4.3×10^4 km^2. The regions were mesoscale in lifetime as well as in size, lasting between 9 and 20 h. Each became well-defined several hours after intense convective cells became organized along the leading edge of the mesoscale system, and then persisted for several hours after the last convective cells had dissipated. In this respect, the areas of horizontally uniform precipitation in Figs. 1–5 apparently resemble those described by Ramana

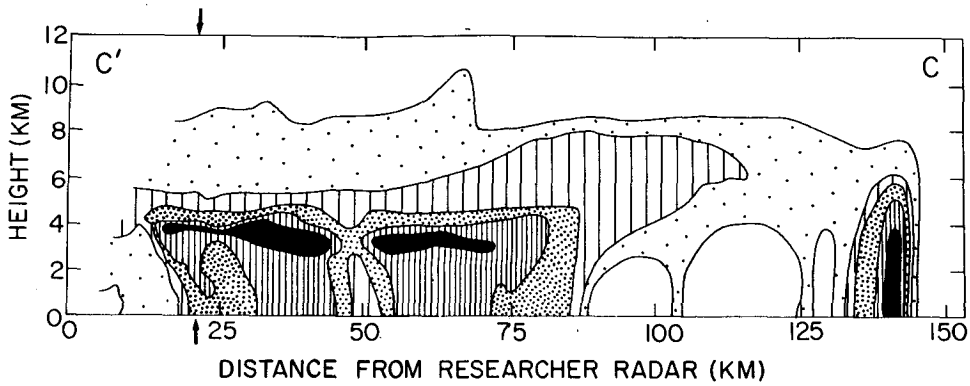

(a)

FIG. 3a. Vertical cross section derived from *Researcher* digital radar data for 2130 GMT 12 September 1974, lying along line C–C′ in Fig. 3b. The outside contour is for the minimum detectable echo, inner contours are for 23, 28, 33 and 38 dBZ, and arrows indicate the vertical profile in Fig. 6c.

Murty *et al.* (1965). They noted that a "well defined bright band appears on the radar towards the declining stage of the precipitation process" in "widespread steady rain."

In our five cases, distinct radar bright bands were observed beneath the 0°C isotherm which was located at ~4.5 km. The increase in reflectivity for precipitation particles falling through the bright band has been attributed largely to the film of liquid water which coats coalesced snowflakes as they melt from the outside (Austin and Bemis, 1950). That snowflakes melt from the outside is consistent with the calculations of Fletcher (1968) which predict the existence of a quasi-liquid surface on ice having a thickness of a few molecular layers at −6°C, increasing to about 10 layers at −1°C. Below the bright band, the decrease in reflectivity is mainly the result of the reduced size of the completely melted precipitation particles and the increase in terminal velocity from values $\lesssim 2$ m s^{-1} for ice particles (Hobbs, 1974, pp. 671–693) to several meters per second for raindrops (Fletcher, 1966, pp. 194–5). The increase in terminal fallspeed spreads the raindrops over a larger volume of air, thus lowering the radar reflectivity below the melting layer.

The five bright bands were themselves horizontally uniform. They were not made irregular by convective updrafts or downdrafts, whose vertical velocities are characteristically greater than the terminal fallspeeds of ice particles. Strong convective updrafts would not have permitted the ice particles to fall through the 0°C isotherm and melt, while convective downdrafts would have spread the melting of the ice particles over a deeper vertical layer, rendering a bright band evident only between the convective cells.

Deep layers of low reflectivity were observed above the 0°C isotherm in each of the areas of horizontally uniform precipitation shown in Figs. 1–5. These low reflectivity values are typical of ice crystals and underscore the importance of the ice phase in the microphysics of the anvil cloud and in the production of horizontally uniform precipitation. The vertical profiles of reflectivity in Fig. 6 show an increase in reflectivity with decreasing height above the melting layer similar to that observed by Lhermitte and Atlas (Battan, 1973, Fig. 10.13). They attributed the increase in reflectivity to ice particle growth, and, especially just above the melting layer, to aggregation of ice crystals. Houze *et al.* (1976) used Doppler radar data and airborne measurements of ice particle type, size and concentration to conclude that ice particles settling in rainbands of

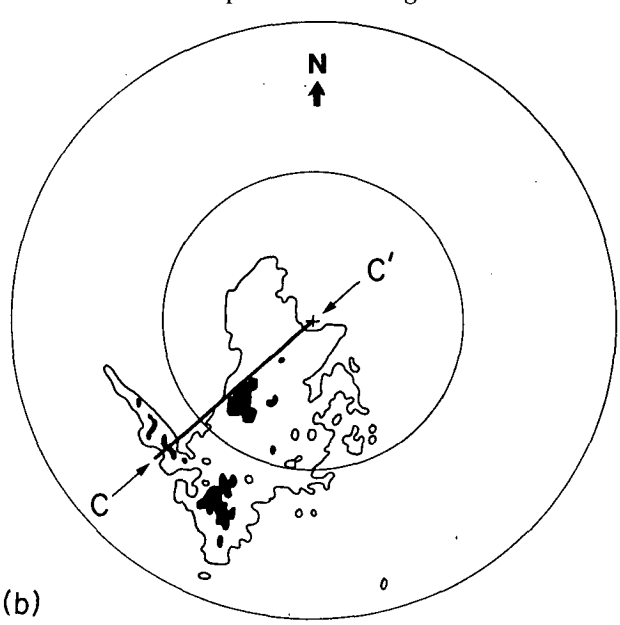

(b)

FIG. 3b. As in Fig. 3a except for horizontal cross section. The outside contour is for the minimum detectable echo, inner contours are for 23, 28, 33, and 38 dBZ, and arrows indicate the vertical profile in Fig. 6c. The outside contour is for the minimum detectable echo, the inner contour is for 38 dBZ or 14 mm h^{-1}, and range marks are at 110 and 220 km.

occluded frontal systems grow first by vapor deposition, and, just above the melting layer, by aggregation and possibly riming. Using Eq. (3) (see Section 4) we obtained maximum ice water concentrations of up to 2.8 g m^{-3} just above the melting layer and concentrations $\lesssim$0.5 g m^{-3} well above the melting layer in Figs. 1–5.

Below the base of the melting layer, the average radar reflectivity in the cross sections of Figs. 1–5 decreased with decreasing height. We attribute this decrease in reflectivity to evaporation as raindrops fall through unsaturated air. That the decrease in reflectivity with decreasing height is not uniform in the five cross sections suggests that at some ranges growth of raindrops by coalescence occurs, or that vertical convergence of precipitation due to decreasing fall velocities of evaporating raindrops permits the liquid water content to decrease less with decreasing height than would be expected from evaporation alone.

In all five cases average precipitation rates at the surface are between 1 and 10 mm h^{-1}. These rates are considerably lower than the 10–100 mm h^{-1} rainfall rates associated with active convective cells. These low rainfall rates, however, can contribute substantially to the water budget of a storm, since they extend over large horizontal areas. Houze (1977) calculated that 40% of the rain that fell in the squall-line system of 4–5 September 1974 (see Fig. 1) could be attributed to the area of horizontally uniform precipitation. Preliminary examination of the cases shown in Figs. 2–5 suggests that this is also true in those situations.

Ramana Murty *et al.* (1965) reported somewhat lower (0.3–1.0 mm h^{-1}) surface rainfall rates below bright bands in India. Since their radar had a wavelength of 3.2 cm, attenuation may have made their observations an underestimate of the true rainfall rates.

4. Cooling in the melting layer

The existence of distinct bright bands in the areas of horizontally uniform precipitation shown in Figs. 1–5 suggests that significant cooling due to the melting of ice crystals is concentrated in a narrow layer in the vicinity of the 0°C isotherm. If we assume, as did Austin and Bemis (1950), that there are no sources or sinks of water in the melting layer, it is possible to obtain from Figs. 1–5 two different estimates of the cooling rates in the layer of air cooled by the melting of falling ice particles. These are calculated using the equations

$$\frac{\Delta T}{\Delta t}=\frac{V_I L_f I}{C_p \rho \Delta z} \tag{1}$$

and

$$\frac{\Delta T}{\Delta t}=\frac{V_R L_f M}{C_p \rho \Delta z}, \tag{2}$$

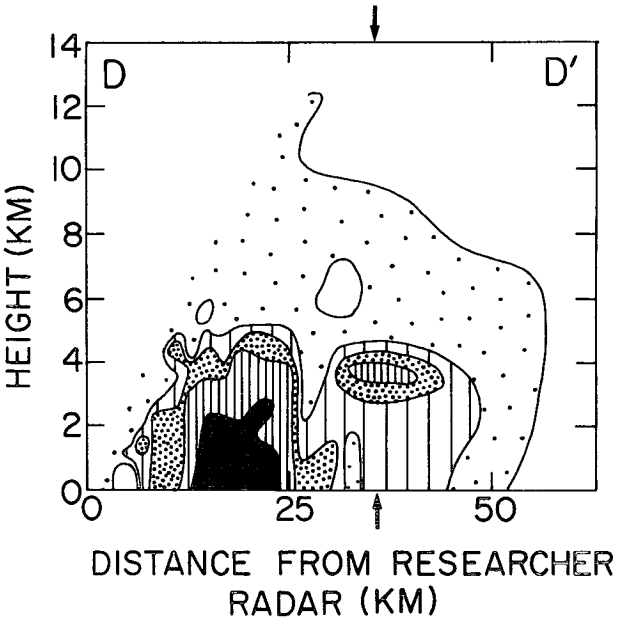

FIG. 4a. Vertical cross section derived from *Researcher* digital radar data for 1000 GMT 16 September 1974, lying along line D–D′ in Fig. 4b. The outside contour is for the minimum detectable echo, inner contours are for 23, 33 and 38 dBZ, and arrows indicate the vertical profile in Fig. 6d.

where L_f is the latent heat of fusion, C_p the specific heat of air at constant pressure, ρ the density of the air, Δz the depth of the melting layer, I the ice water

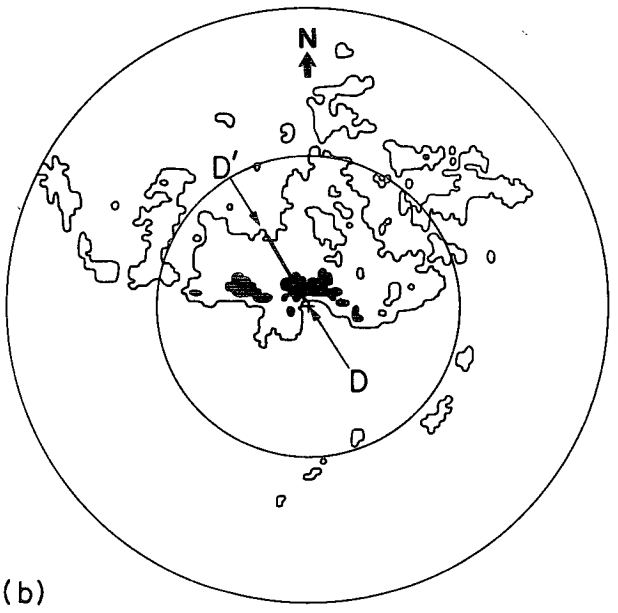

FIG. 4b. As in Fig. 4a except for horizontal cross section. The outside contour is for the minimum detectable echo, the inner contour is for 38 dBZ or 14 mm h^{-1}, and range marks are at 110 and 220 km.

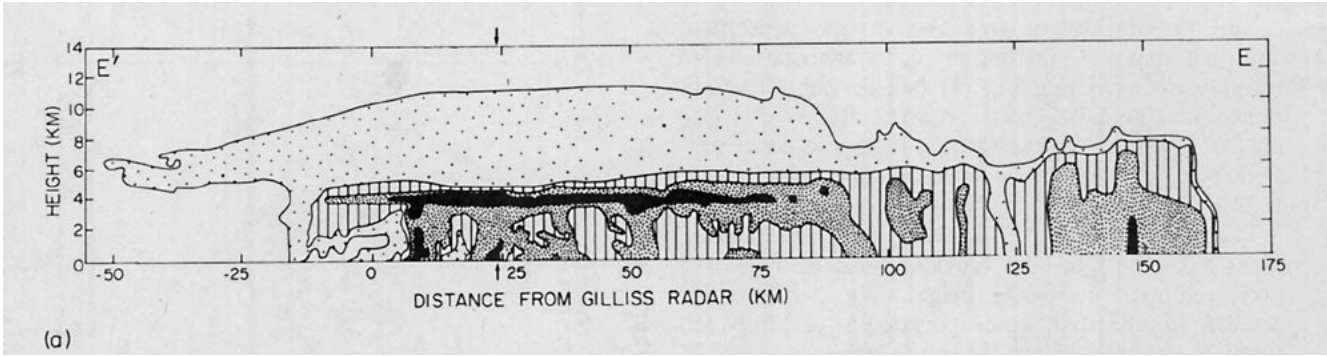

FIG. 5a. Vertical cross section derived from *Gilliss* digital radar data for 1600 GMT 5 September 1974, lying along line E–E′ in Fig. 5b. The outside contour is for the minimum detectable echo, inner contours are for 26, 31 and 36 dBZ, and arrows indicate the vertical profile in Fig. 6e.

content (kilograms of solid precipitation particles per cubic meter of air) evaluated at the top of the melting layer and M the liquid water content (kilograms of liquid precipitation particles per cubic meter of air) at the base of the melting layer. These equations were derived by assuming that the mass flux of precipitation particles, IV_I in (1) and MV_R in (2), acts as a heat source for the mass of air contained in the layer through which the melting hydrometeors pass. The cooling rates are directly proportional to the terminal velocities of the precipitation particles. The value for aggregate snowflakes ($V_I = 1.5$ m s^{-1}) is based on data discussed by Hobbs (1974), and the value for raindrops ($V_R = 6$ m s^{-1}) was obtained from Fletcher (1966).

The following expressions were assumed for ice water content (I) and liquid water content (M):

$$I = 8.0\times10^{-3}\, Z_I^{0.61}, \tag{3}$$

$$M = 5.5\times10^{-4}\, Z^{0.80}, \tag{4}$$

where Z_I and Z are the radar reflectivities (mm^6 m^{-3}) of ice and liquid precipitation, respectively. Eq. (3) is based on airborne measurements of the size distributions of aggregate snowflakes (Herzegh and Hobbs, 1978).[3] The ice water contents determined using (3) agree to within a factor of 3 with those obtained using the relationships listed by Battan (1973, p. 88) and determined by Sekhon and Srivastava (1970) based on observations of ice crystals at ground level. Eq. (4) is based on measurements of raindrop size distributions obtained on board the *Gilliss* during GATE (Austin and Geotis, 1978, personal communication).

We determined the base and top of the melting layer and the radar reflectivities there by constructing the vertical profiles of reflectivity for each case shown in Fig. 6 at ranges where the vertical resolution of the radar data permitted the bright bands to be especially well-resolved. The profiles were then compared to the vertical profile of reflectivity obtained through stratiform precipitation by Lhermitte and Atlas (Battan, 1973, Fig. 10.13). Using simultaneous Doppler radar measurements of precipitation fallspeeds, they were able to define clearly the melting layer by the sharp increases in speed of falling precipitation particles at the top and at the bottom of the layer. On their reflectivity profile, the top of the melting layer occurred where the curvature of the profile changed sign, and the base of the melting layer was located where the curvature of the reflectivity profile changed abruptly. We applied these criteria to the vertical profiles in Fig. 6 to obtain Z_T and Z_B, the top and the base of the melting layer, respectively. In some cases, these criteria were difficult to apply. For example, evaporation below the bright band made the base of the melting layer difficult to discern in Fig. 6b.

Applying the shape criteria to each of the five cases yielded values of Z_T and Z_B that were consistent from

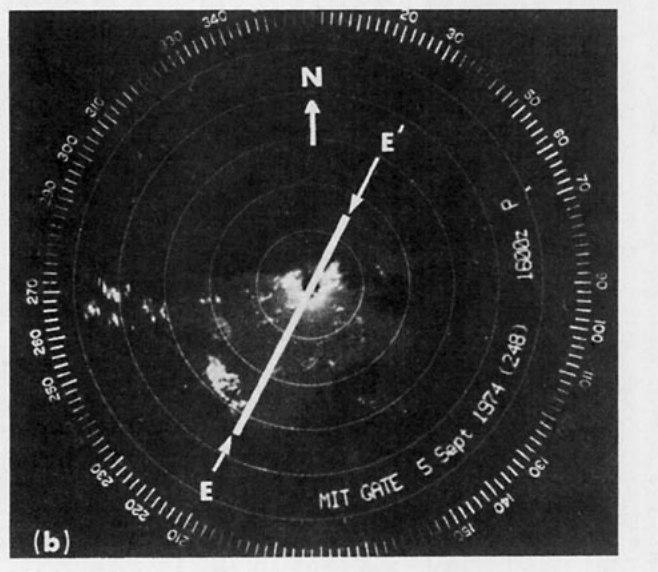

FIG. 5b. As in Fig. 5a except for horizontal cross section. The shading thresholds are for 11 dBZ or 0.1 mm h^{-1} (gray) and 36 dBZ or 10 mm h^{-1} (white), and range marks are at intervals of 50 km.

[3] Eq. (3) above is equivalent to Eq. (2) of Herzegh and Hobbs (1978) when 6.7 dBZ is added to their effective reflectivity Z_e, since Z_e was calculated using the complex index of refraction for water.

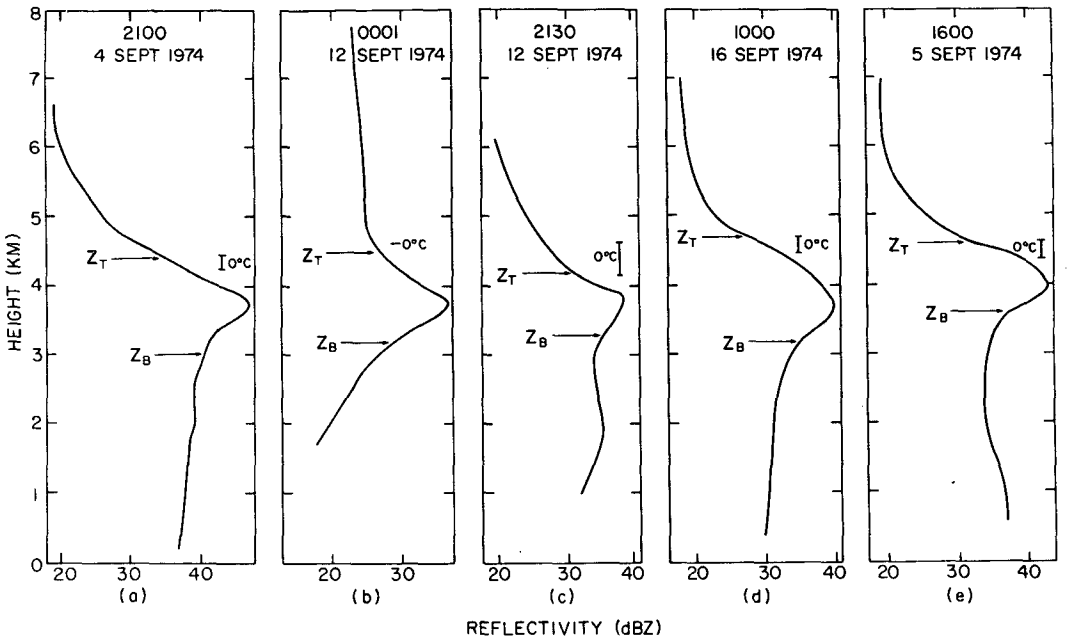

FIG. 6. Vertical profiles of radar reflectivity at ranges indicated by arrows in (a) Fig. 1a, (b) Fig. 2a, (c) Fig. 3a, (d) Fig. 4a, (e) Fig. 5a. Z_T and Z_B indicate the top and the base of the melting layer, respectively. Estimates of the height of the 0°C isotherm, as derived from rawinsonde data, are indicated as a range when more than one sounding was used.

case to case. The location of the 0°C isotherm provided another check on our estimates of the top of the melting layer. Rawinsondes as closely spaced as possible in position and time to the area of horizontally uniform precipitation were used to obtain estimates of the height of the 0°C isotherm in each case (Fig. 6). Where more than one sounding was used, the range of values for the height are indicated. In no case is our estimate for Z_T more than 0.1 km outside the range of estimated height for the 0°C isotherm. Our values of Δz, the depth of the melting layer (listed in Table 1), also compare well with melting-layer depths of 0.9–1.2 km estimated by Biswas *et al.* (1962).

Good agreement was obtained between the cooling rates calculated using (1) and (3) and those calculated using (2) and (4) (Table 1). Exact agreement was not expected because of uncertainties in precipitation fallspeeds, the empirical nature of relationships (3) and (4), and the possibility that evaporation or particle growth occurs in the melting layer.

As will be discussed in Section 6, the cooling of the air due to melting in all five cases appears to be sufficiently large to have important dynamic consequences in the region of horizontally uniform precipitation.

5. Particle size distributions above and below the melting layer

Houze *et al.* (1979) found that airborne measurements of the size spectra of ice particles in frontal clouds associated with mesoscale rainbands tend to follow the relationship suggested by Marshall and Palmer (1948), i.e.,

$$N(D)=N_0\exp(-\lambda D), \tag{5}$$

where $N(D)dD$ is the number of particles per unit volume of air with diameters between D and $D+dD$, and N_0 and λ are constants. They concluded that the size distribution of ice particles with diameters $\gtrsim 1$ mm was described by (5) over a wide range of temperatures, and that λ and N_0 both decrease with increasing temperature.

Fig. 7 shows particle size distributions derived from the results of Houze *et al.* (1979) for temperatures of −10 and 0°C. The −10°C distribution corresponds to an altitude of about 6.4 km (Fig. 6). The 0°C distribution corresponds to the top of the melting layer, at an altitude of about 4.5 km. This distribution has a smaller

TABLE 1. Cooling rates ($\Delta T/\Delta t$) in the melting layer of depth Δz, evaluated using the ice water content (I) at the top of the melting layer (Z_T) and using the liquid water content (M) at the base of the melting layer (Z_B) for the vertical reflectivity profiles (Fig. 6) derived from Figs. 1–5.

Figure	Z_T (km)	I (g m^{-3})	Z_B (km)	M (g m^{-3})	Δz (km)	$\Delta T/\Delta t$ (K h^{-1}) I	M
1	4.4	2.8	3.0	1.12	1.4	−4.4	−7.0
2	4.5	0.9	3.2	0.11	1.3	−1.5	−0.8
3	4.2	1.8	3.3	0.35	0.9	−4.5	−3.4
4	4.7	1.0	3.2	0.35	1.5	−1.6	−2.1
5	4.6	1.8	3.6	0.52	1.0	−4.2	−4.7

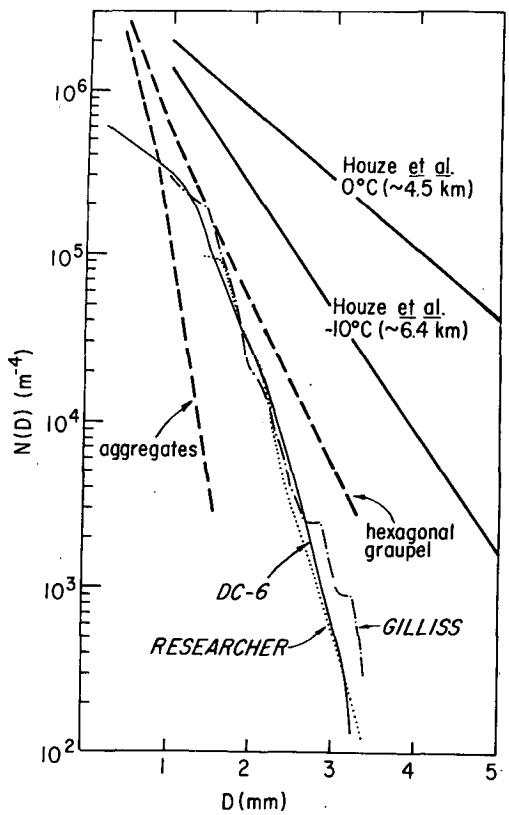

FIG. 7. Particle size distributions 1) for ice particles as reported by Houze *et al.* (1979) in precipitating clouds above and at the top of the melting layer (heavy solid lines); 2) for raindrops as measured during GATE by disdrometers on board the *Researcher* (dotted line) and *Gilliss* (dash-dotted line) and by foil impactor on the DC-6 aircraft (light solid line), when rainfall rates were in the range 1–10 mm h^{-1}; and 3) for rain as calculated using the distribution from Houze *et al.* (1979) at 0°C and, first, assuming melting of hexagonal graupel and second, melting of aggregates of densely rimed dendrites or radiating assemblages of dendrites (heavy dashed lines). D indicates particle diameter.

slope than the −10°C distribution, reflecting an increase in the relative number of large ice particles at 0°C. Houze *et al.* (1979) attribute this change in slope to growth of the particles by collection. Since aggregation can produce particles with maximum dimensions in excess of 3 mm at temperatures higher than −15°C, and the largest aggregates (up to ~14 mm) are observed at temperatures just above 0°C (Hobbs, 1974, Fig. 10.4), the increase in the number of large particles from −10–0°C is probably due to aggregation.

Below the melting layer, we obtained estimates of the average concentrations of raindrops of different sizes from airborne drop size measurements collected during GATE at cloud base from the NOAA DC-6 aircraft and at the surface from the disdrometers on board the *Researcher* and *Gilliss*. Using the data compiled by Cunning and Sax (1977a) and Austin and Geotis (1979) we derived the three curves shown in Fig. 7. The DC-6 curve represents the concentrations of raindrops in different size categories averaged over the 50 samples whose precipitation rates were between 1 and 10 mm h^{-1}. The *Researcher* curve is based on 80 samples and the *Gilliss* curve is based on 30 samples whose precipitation rates fell in the same interval. The curves agree well for drops having diameters of about 1.5 mm and above. The *Researcher* and *Gilliss* disdrometers failed to detect drops in the smaller size categories because of shipboard background noise (Cunning and Sax, 1977a).

In the absence of direct observations of ice particle type in horizontally uniform precipitation during GATE, we used the 0°C particle size distribution (Fig. 7) derived from Houze *et al.* (1979) together with relationships between fallspeeds, masses and types of ice crystals from Locatelli and Hobbs (1974) to indicate the type of ice particles which, when melted, would produce raindrop size distributions corresponding to those obtained from the *Researcher*, *Gilliss* and DC-6 data. For two different assumed populations of ice crystal type, we calculated raindrop size spectra using

$$N(D_w)=\frac{N(D_s)D_sV_s}{D_wV_w}, \tag{6}$$

$$V_s=aD_s^b, \tag{7}$$

$$M_s=cD_s^d, \tag{8}$$

where $N(D_w)$ and $N(D_s)$ are the number of particles per unit volume of air per unit interval of particle diameter for rain and snow, respectively, D_s is ice particle diameter, D_w the raindrop diameter, V_s the terminal velocity of the ice crystal, V_w the raindrop terminal velocity and M_s the mass of the ice particle. Eq. (6) expresses the size spectrum of melted hydrometeors in terms of the size spectrum of frozen hydrometeors, and takes into account the effects of the differences in fallspeeds and diameters between the frozen and melted particles. In (7) and (8), obtained from Locatelli and Hobbs (1974), the quantities a, b, c and d vary with ice particle type, and have units of milligrams for M_s, millimeters for D_s and meters per second for V_s. Raindrop terminal velocities were obtained from Fletcher (1966).

Assuming that the ice particles at 0°C were aggregates of densely rimed dendrites or radiating assemblages of dendrites, with $a=0.79$, $b=0.27$, $c=0.037$ and $d=1.9$ (Locatelli and Hobbs, 1974), produced a size distribution with values of $N(D_w)$ much lower than observed values except for the smallest particles. The assumption that the ice particles at 0°C were hexagonal graupel, with $a=1.1$, $b=0.57$, $c=0.044$, $d=2.9$ (Locatelli and Hobbs, 1974), produced a distribution of raindrops (Fig. 7) with the values of $N(D_w)$ somewhat higher than were observed.

Of the two assumptions, that of hexagonal graupel agreed best with the observed concentrations of rain-

drops. This suggests that substantial quantities of supercooled cloud liquid water are present above the 0°C isotherm to account for sufficient riming to produce graupel. The presence of enough supercooled liquid water to produce heavy riming and graupel is consistent with the presence of mesoscale uplift in the anvil cloud. Graupel, composed of an ice particle coated with a heavy deposit of rime, is quite distinct from hail, with its laminar structure and smooth glazed surface. The extreme case of growth by riming that produces hail can occur only in the presence of intense convective updrafts of tens of meters per second (Hobbs, 1974, p. 645), which would produce quite different radar reflectivity patterns than we have found in regions of horizontally uniform precipitation. Nowhere in any of the five cases studied (Figs. 1–5) were the reflectivity values at any level high enough (Battan, 1973, pp. 185–187) to suspect the presence of hail, either in the region of horizontally uniform precipitation or in the accompanying area occupied by intense convective cells.

6. Evaporative cooling and subsidence below the melting layer

The amount of liquid water lost to evaporation beneath the melting layer can be a significant fraction of the total amount of water melted in the melting layer. Table 2 lists for each of Figs. 1–5 the change in the average precipitation liquid water content in the region of horizontally uniform precipitation between the 2.5 and 0.5 km levels. Except in Fig. 5, the observed change was >25% in each case. These changes can be attributed to evaporation beneath the melting layer.

Such large amounts of liquid water lost to evaporation suggest that significant cooling occurs beneath the melting layer in regions of horizontally uniform precipitation. For each of Figs. 1–5, the cooling rate due to evaporation in the layer between 2.5 and 0.5 km was calculated using

$$\frac{\Delta T}{\Delta t}=\frac{V_r L_v \Delta \bar{M}}{C_p \rho \Delta z}, \tag{9}$$

where L_v is the latent heat of vaporization of air, Δz is 2 km, and $\Delta\bar{M}$ is the change in average precipitation liquid water content from 2.5–0.5 km. This layer was chosen because its top lies beneath the base of the melting layer for all five cases, and because its base nearly coincides with the lowest tilt angle of the radar data. Table 2 lists the ranges over which the liquid water content was averaged at each level to compute $\Delta\bar{M}$ for each case. The table also lists the computed cooling rates. In four cases (Figs. 1–4) the cooling rates due to evaporation are comparable in magnitude to the cooling rates computed in Section 4 due to melting in the vicinity of the bright band. In the fifth case (Fig. 5), the cooling due to evaporation in the 0.5–2.5 km layer is more than an order of magnitude smaller than that computed for melting in the vicinity of the bright band.

TABLE 2. Fraction of liquid water content evaporated and average cooling rates ($\Delta T/\Delta t$) due to evaporation in the layer between 2.5 and 0.5 km and precipitation rates at 0.5 km computed from Figs. 1–5. $\Delta\bar{M}$ is the difference between the average liquid water content ($\bar{M}$) at 2.5 km and at 0.5 km.

Figure	Ranges (km) used to compute $\Delta\bar{M}$	$\frac{\Delta\bar{M}}{\bar{M}}$ at 2.5 km	$\frac{\Delta T}{\Delta t}$ (K h^{-1})	Precipitation rate (mm h^{-1}) corresponding to $\bar{M}$ at 0.5 km
1	−14 to −4; 7 to 91	0.38	−6.2	8.9
2	9 to 33	0.75	−0.8	0.3
3	15 to 49	0.27	−2.1	5.2
4	33 to 51	0.40	−1.6	2.3
5	−51 to −7; 7 to 37	0.04	−0.2	4.5

Houze (1977) deduced from wind and thermodynamic observations that the region occupied by horizontally uniform precipitation below the melting level in the squall-line system shown in Fig. 1 contained a mesoscale downdraft. Zipser (1969, 1977) made a similar inference with respect to several other cases of tropical squall lines, including the one shown in Fig. 3, and suggested that evaporative cooling from falling rain could drive such a downdraft.

Aircraft observations in the region of horizontally uniform precipitation of a non-squall convective system led Leary and Houze (1979) to infer that intense convection in non-squall situations can also produce mesoscale, evaporatively driven downdrafts. Brown (1979), using a hydrostatic numerical model with a parameterization of microphysical processes, and initial conditions chosen for their resemblance to the large-scale environment of a tropical squall-line system, was able to simulate an evaporatively driven mesoscale downdraft beneath the anvil cloud. These observations and modeling results are consistent with our calculations of significant amounts of evaporation accompanied by cooling rates of up to several degrees per hour beneath the melting layer in regions of horizontally uniform precipitation.

Although Brown (1979) has been able to simulate mesoscale downdrafts numerically without including cooling due to melting, the position of the bright band near the base of the anvil cloud and our calculations of cooling rates due to melting of up to several degrees per hour suggest that melting may cooperate with evaporation both in maintaining and in initiating the mesoscale downdraft.

7. Conclusions

The schematic shown in Fig. 8 depicts our synthesis of observations from five examples of horizontally uniform precipitation in and beneath the anvil clouds of deep tropical convection. The nimbostratus anvil

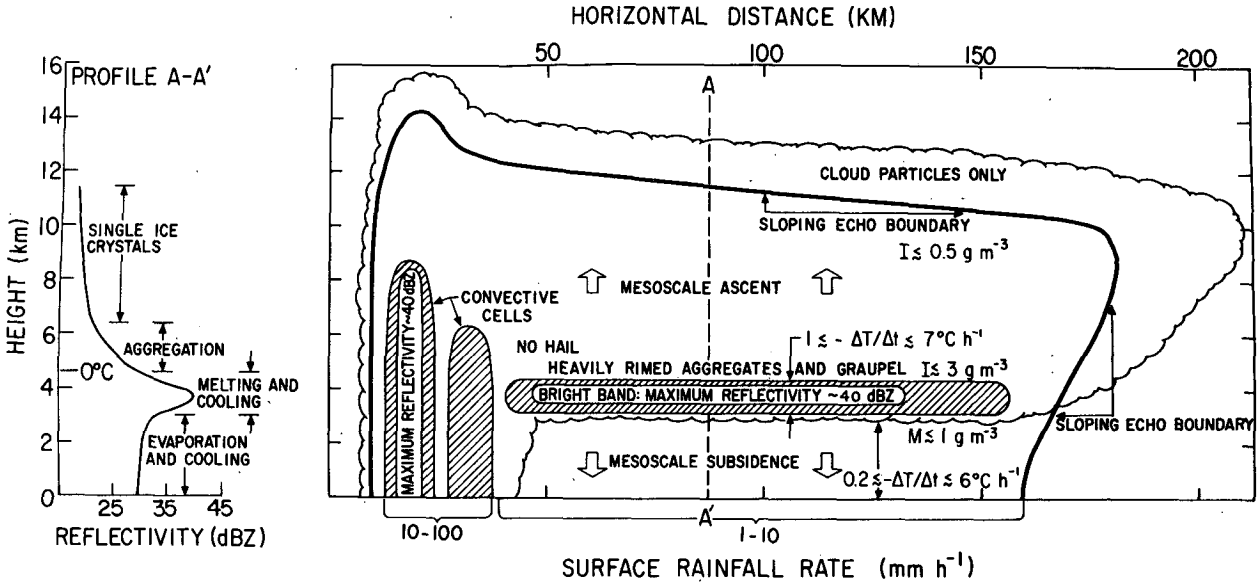

FIG. 8. Schematic vertical cross section and vertical profile of radar reflectivity (along dashed line A–A' in the cross section) in horizontally uniform precipitation associated with an anvil cloud. The anvil cloud occurs to the rear of intense convective cells propagating in the direction from right to left in the figure. The dark solid line is the contour of minimum detectable radar echo, lighter solid lines and shading indicate contours of higher reflectivity, and the scalloped line indicates the cloud boundary.

cloud extends from the 600–700 mb (3.2–4.4 km) level to 12 km or higher. The top of the anvil cloud exceeds the upper boundary of the radar reflectivity pattern, which delineates the boundary above which precipitation-sized particles cannot be detected. The sloping echo boundary, both at the top of the anvil cloud and to its rear, where the cloud extends many kilometers to the rear of the radar echo, indicates dissipation in the trailing portions of the anvil cloud. The longevity of the anvil cloud (between 9 and 20 h for our five cases), its large horizontal dimension and the large quantities of precipitation associated with it are all consistent with the presence of mesoscale uplift within the anvil cloud.

The anvil cloud and the area of horizontally uniform precipitation form to the rear of deep intense cellular convection characterized by strong horizontal reflectivity gradients and surface rainfall rates of 10–100 mm h^{-1}. In contrast, the reflectivity pattern in and beneath the anvil cloud is characterized by its striking horizontal uniformity and surface rainfall rates of 1–10 mm h^{-1}.

Vertical profiles of reflectivity in the region of horizontally uniform precipitation show a maximum just below the 0°C isotherm, where the radar bright band outlines the melting level. Melting accounts for cooling rates of up to several degrees per hour in this layer. Just above the melting layer, ice water contents of up to ~3 g m^{-3} of small graupel or heavily rimed aggregates are observed in the region of aggregation, where the reflectivity increases with decreasing height. Further aloft, a deep layer of low reflectivity values extends to the 10–12 km level.

Extensive evaporation can occur in precipitation falling from the base of the anvil cloud to the surface. The cooling rates associated with this evaporation can be as high as several degrees per hour, and are consistent with the presence of a mesoscale, evaporatively driven downdraft beneath the anvil cloud. The location of the bright band, together with cooling rates there due to melting which are comparable to those produced by evaporation below the anvil cloud, suggest that cooling due to melting plays a role in the initiation and maintenance of the mesoscale downdraft.

Acknowledgments. The following GATE scientists provided the authors with data: Dr. Geoffrey L. Austin, Dr. Pauline M. Austin, Mr. Spiros G. Geotis, Dr. Michael D. Hudlow, Mr. Frank D. Marks, Dr. David W. Martin, Mr. Ernest E. Recker, Prof. Richard J. Reed and Dr. David Suchman. The figures were drafted by Mrs. Kay Moore.

This research was supported by the Global Atmospheric Research Program, National Science Foundation, and the U.S. GATE Project Office, National Oceanic and Atmospheric Administration, Grant ATM74-14830.

REFERENCES

Acheson, D., 1976: Documentation for GATE B-scale rawinsondes. GATE Processed and Validated Data, 21 pp. [Available from World Data Center-A, National Climatic Center, Asheville, NC 28801.]

Atlas, D., K. R. Hardy, R. Wexler and R. J. Boucher, 1963: On the origin of hurricane spiral bands. *Geophys. Int.*, 3, 123–132.

Austin, P. M., and A. C. Bemis, 1950: A quantitative study of the

"bright band" in radar precipitation echoes. *J. Meteor.*, **7**, 145–151.

——, and S. G. Geotis, 1979: Raindrop sizes and related parameters for GATE. *J. Appl. Meteor.*, **18**, 569–575.

Battan, L. J., 1973: *Radar Observations of the Atmosphere.* The University of Chicago Press, 324 pp.

Biswas, K. R., Bh. V. Ramana Murty and A. K. Roy, 1962: Freezing rain at Delhi and associated melting band characteristics. *Indian J. Meteor. Geophys.*, **13** (Spec. issue), 137–142.

Brown, J. M., 1979: Mesoscale unsaturated downdrafts driven by rainfall evaporation: A numerical study. *J. Atmos. Sci.*, **36**, 313–338.

Cunning, J. B., and R. I. Sax, 1977a: Raindrop size distributions and *Z-R* relationships measured on the NOAA DC-6 and the ship *Researcher* within the GATE B-scale array. NOAA Tech. Memo. ERL-WMPO-37, 136 pp. [NTIS PB-269 659/961].

——, and ——, 1977b: A *Z-R* relationship for the GATE B-scale array. *Mon. Wea. Rev.*, **105**, 1330–1336.

EDS, 1975: *GATE Data Catalog.* Environmental Data Service, NOAA, Washington, DC. [Available from Environmental Data Service, Federal Building, Asheville, NC 28801.]

Fletcher, N. H., 1966: *The Physics of Rainclouds.* Cambridge University Press, 390 pp.

——, 1968: Surface structure of water and ice. II. A revised model. *Phil. Mag.*, **18**, 1287–1300.

Herzegh, P. H., and P. V. Hobbs, 1978: Generating cells and precipitation growth in mesoscale rainbands. *Preprints Conf. Cloud Physics and Atmospheric Electricity*, Issaquah, Amer. Meteor. Soc., 284–291.

Hobbs, P. V., 1974: *Ice Physics.* Oxford University Press, 837 pp.

Houghton, H. G., 1968: On precipitation mechanisms and their artificial modification. *J. Appl. Meteor.*, **7**, 851–859.

Houze, R. A., Jr., 1975: Squall lines observed in the vicinity of the *Researcher* during Phase III of GATE. *Preprints 16th Radar Meteorology Conf.*, Houston, Amer. Meteor. Soc., 206–209.

——, 1977: Structure and dynamics of a tropical squall-line system. *Mon. Wea. Rev.*, **105**, 1540–1567.

——, and C.-P. Cheng, 1977: Radar characteristics of tropical convection observed during GATE: Mean properties and trends over the summer season. *Mon. Wea. Rev.*, **105**, 964–980.

——, J. D. Locatelli and P. V. Hobbs, 1976: Dynamics and cloud microphysics of the rainbands in an occluded frontal system. *J. Atmos. Sci.*, **33**, 1921–1936.

——, P. V. Hobbs, P. H. Herzegh and D. B. Parsons, 1979: Size distributions of precipitation particles in frontal clouds. *J. Atmos. Sci.*, **36**, 156–162.

Leary, C. A., and R. A. Houze, Jr., 1979: The structure and evolution of convection in a tropical cloud cluster. *J. Atmos. Sci.*, **36**, 437–457.

Locatelli, J. D., and P. V. Hobbs, 1974: Fall speeds and masses of solid precipitation particles. *J. Geophys. Res.*, **79**, 2185–2206.

Marshall, J. S., and W. McK. Palmer, 1948: The distribution of raindrops with size. *J. Meteor.*, **5**, 165–166.

Payne, S. W., and M. M. McGarry, 1977: The relationship of satellite inferred convective activity to easterly waves over West Africa and the adjacent ocean during Phase III of GATE. *Mon. Wea. Rev.*, **105**, 413–420.

Ramana Murty, Bh. V., A. K. Roy and K. R. Biswas, 1965: Radar echo intensities below bright band. *J. Atmos. Sci.*, **22**, 91–94.

Sekhon, R. S., and R. C. Srivastava, 1970: Snow size spectra and radar reflectivity. *J. Atmos. Sci.*, **27**, 299–307.

Zipser, E. J., 1969: The role of organized unsaturated convective downdrafts in the structure and decay of an equatorial disturbance. *J. Appl. Meteor.*, **8**, 799–814.

——, 1977: Mesoscale and convective-scale downdrafts as distinct components of squall-line circulation. *Mon. Wea. Rev.*, **105**, 1568–1589.

Zwack, P., and C. Anderson, 1970: 25 July 1969: Showers and continuous precipitation. *Preprints 14th Radar Meteor. Conf.*, Tucson, Amer. Meteor. Soc. 335–338.